Natural Resources Canada | Ressources naturelles Canada

GEOLOGICAL SURVEY OF CANADA
OPEN FILE 8928

RADARSAT constellation mission (RCM) InSAR preliminary observations of slope movements in British Columbia, Alberta, and Nunavut

B.-H. Choe, A. Blais-Stevens, S. Samsonov, and J. Dudley

2022

Canada

ISSN 2816-7155
ISBN 978-066-0-46069-7
Catalogue No. M183-2/8928E-PDF

GEOLOGICAL SURVEY OF CANADA
OPEN FILE 8928

RADARSAT constellation mission (RCM) InSAR preliminary observations of slope movements in British Columbia, Alberta, and Nunavut

B.-H. Choe, A. Blais-Stevens, S. Samsonov, and J. Dudley

2022

Permanent link: https://doi.org/10.4095/331099

This publication is available for free download through GEOSCAN (http://geoscan.nrcan.gc.ca/).

Recommended citation

Choe, B.-H., Blais-Stevens, A., Samsonov, S., and Dudley, J., 2022. RADARSAT constellation mission (RCM) InSAR preliminary observations of slope movements in British Columbia, Alberta, and Nunavut; Geological Survey of Canada, Open File 8928, 15 p. https://doi.org/10.4095/331099

Publications in this series have not been edited; they are released as submitted by the author.

1. Introduction

Landslides are one of the most common natural hazards in western Canada, which have resulted in significant fatalities and damage to infrastructure. British Columbia (BC) has recorded the largest number of fatalities in Canada (i.e., ~377 from the records since 1880) caused by rockfalls, rock slides, rock avalanches, debris flows, etc. (Blais-Stevens, 2020; 2022). As an example, annual costs to repair and mitigate the damage to infrastructure are estimated at 281 to 450M dollars for the western Canada sedimentary basin alone (Porter et al., 2019). In BC, record breaking summer temperatures, forest fires, extreme rainfall, frequent flooding, and deglaciation over mountainous areas with changing climate have increased the risk of landslides (CBC News a, b and c, 2021; CTV news, 2021). It is expected that the costs of infrastructure repairs will be in the billion dollar range.

Interferometric Synthetic Aperture Radar (InSAR) has been extensively used for monitoring ground deformation caused by natural disaster (e.g. earthquakes, volcanos, landslides) or anthropogenic activities (e.g., mining, induced seismicity; Singhroy et al. 2020). Canada has launched three spaceborne SAR missions (i.e., RADARSAT-1 in 1995, RADARSAT-2 in 2007, and RADARSAT Constellation Mission (RCM) in 2019). While the RADARSAT-1 and RADARSAT-2 missions launched a single C-band SAR satellite, the RCM launched a trio of C-band SAR satellites with 4-day revisit capability, which increase the opportunity to detect rapid temporal changes.

The Geological Survey of Canada (GSC)'s Public Safety Geoscience Program (PSGP) has collaborated with the Canada Centre for Remote Sensing (CCRS) to assess the performance of new RCM data for monitoring slope movements. The PSGP has the mandate to study natural hazards and provide baseline geoscience information to help stakeholders and decision-makers mitigate against potential risk. This report provides preliminary results observed from new RCM InSAR data acquired over 21 sites in British Columbia (BC), Alberta (AB), and Nunavut (NU) from April 2020, by comparing them with RADARSAT-2 and Sentinel-1 observations in some cases. Based on the preliminary observations, the advantages and limitations of RCM InSAR for landslide monitoring and some guidelines for future operational plans are suggested.

2. Study areas and RCM data

This work investigated 13 sites in BC, two sites in AB, and six sites in NU that are located close to communities and/or infrastructure, some of which have past records or potential of slope movements (Figure 1). A total of 1235 RCM single look complex (SLC) images of HH polarization (ascending: 514, descending: 721) were acquired from April 2020 to September 2021 (see Appendix). Most of them were acquired with 3 m very-high-resolution and/or 5 m high-resolution modes. The 1 m spotlight mode acquisitions and 4-day interval acquisitions were very limited at the initial operational stage.

3. DInSAR processing

SAR SLC products provide the amplitude and phase information from radar signals transmitted and backscattered from a target surface. The InSAR technique uses the phase difference between two SAR acquisitions caused by ground deformation. Given the wavelength of C-band SAR (i.e., 5.6 cm in wavelength), the phase difference is measured at mm to cm scales. After mitigating the contributions on the phase difference from non-deformational sources (e.g. Earth's curvature, topography, atmospheric noise), the phase difference modulated in 2π can be unwrapped into the amount of displacements. The differential InSAR (i.e., DInSAR, removing the topographic phase

with a digital elevation model) processing was performed with the RCM Data Utilization and Applications Program (DUAP)-InSAR processor to provide on-demand value-added geospatial products for ground deformation on Natural Resources Canada (NRCan)'s new geospatial data platform (i.e., Earth Observation Data Management Systems (EODMS)), available at https://www.eodms-sgdot.nrcan-rncan.gc.ca. The selected parameters for DInSAR processing are as follows (see Dudley and Samsonov (2020) for more details),

- Spatial averaging (i.e., multilooking): 2
- Product enhancement (i.e., filtering): Medium
- Digital Elevation Model (i.e., for topographic phase removal and georeferencing): CDEM (i.e., Canadian Digital Elevation Model)

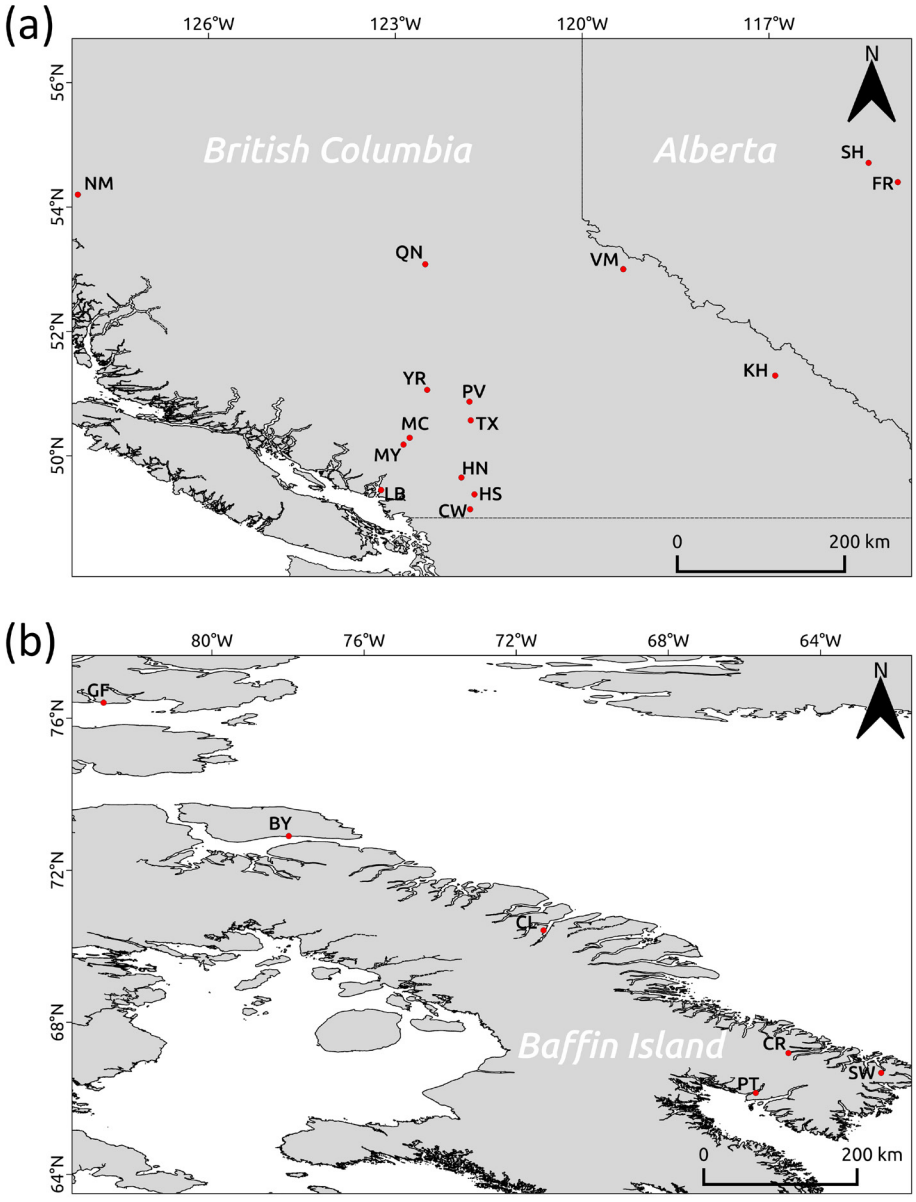

Figure 1. (a) Site locations in BC and AB. (b) Site locations in NU. Abbreviations: NM=Nimbus Mountain; QN=Quesnel; VM=Valemount; YR=Yalakom River; PV=Pavilion; TX=Texas Creek; MC= Mount Currie; MY=Mystery Creek; HN=Harrison Lake North; HS=Harrison Lake South; LB=Lions Bay; CW=Chilliwack; KH=Kicking Horse; SW=Swan Hills; FR=Freeman River; GF=Grise Fiord; BY=Bylot; CL=Clyde River; CR=Coronation; PT=Pangnirtung; SW=Southwind.

4. Results

4. 1. Yalakom River and surrounding areas, BC

Slope movements were observed from well-exposed surfaces with minimal vegetation in Yalakom River and its surrounding areas. Figure 2 shows the examples of slope movements observed by RCM. These are slow-moving earthflows and RCM measured the line-of-sight (LOS) displacements at < ~3 cm over ~2 months in the summer of 2020 (Choe et al., 2021). Two-dimensional (i.e., east-west, vertical) time-series analyses with Sentinel-1 ascending and descending data collected from 2017 to 2021 also confirmed the earthflow movements, which were measured to be up to ~15 cm/year in the east-west direction (Figure 3). In addition to previously reported earthflows (Bovis & Jones, 1992) such as, Red Mountain and Yalakom River earthflows, numerous other relatively small earthflows were detected with RCM and Sentinel-1 in this region. Higher spatial (< 5 m) and temporal (up to 4-day revisit) resolutions of RCM showed great potential for detecting small slope movements within a few hundred metres (e.g. see the full fringe within ~300 m captured by RCM in Figure 2e). The interferograms have been draped over Google earth imagery.

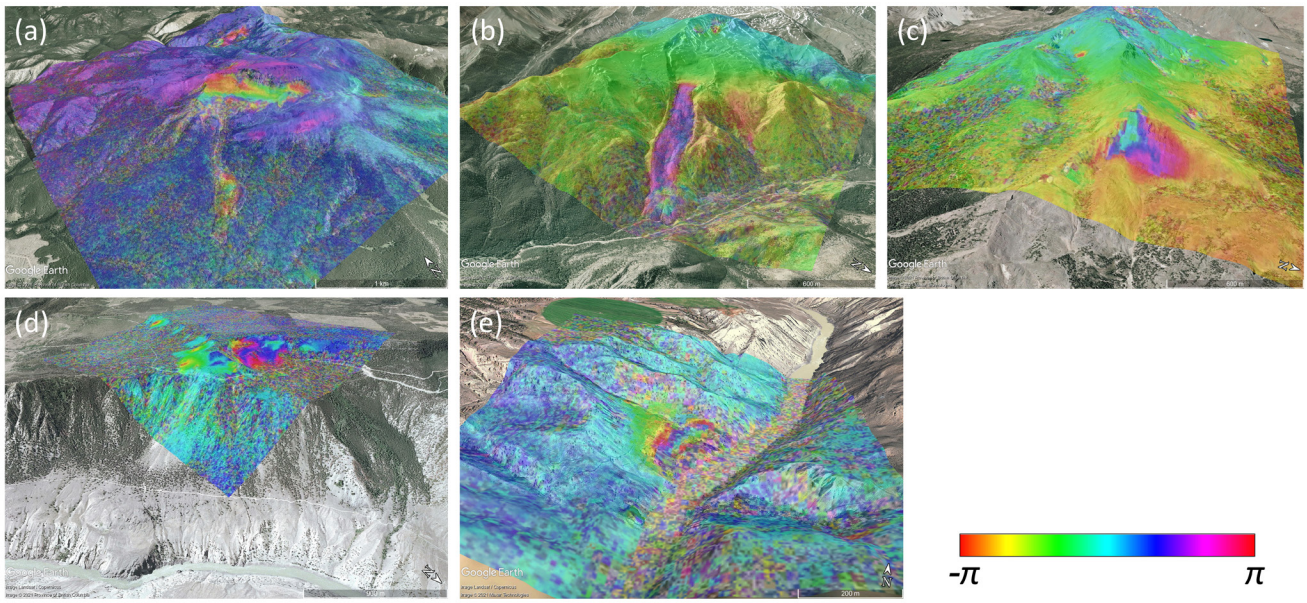

Figure 2. RCM (5M18, 5M23) DInSAR interferograms of 20200626-20200906 rendered on Google Earth imagery, modified from Choe et al. (2021). (a) Site 4 (i.e., Red Mountain), (b) Site 5 (i.e., Yalakom River), (c) Site 6, (d) Site 8, and (e) Site 9 in Choe et al. (2021), respectively.

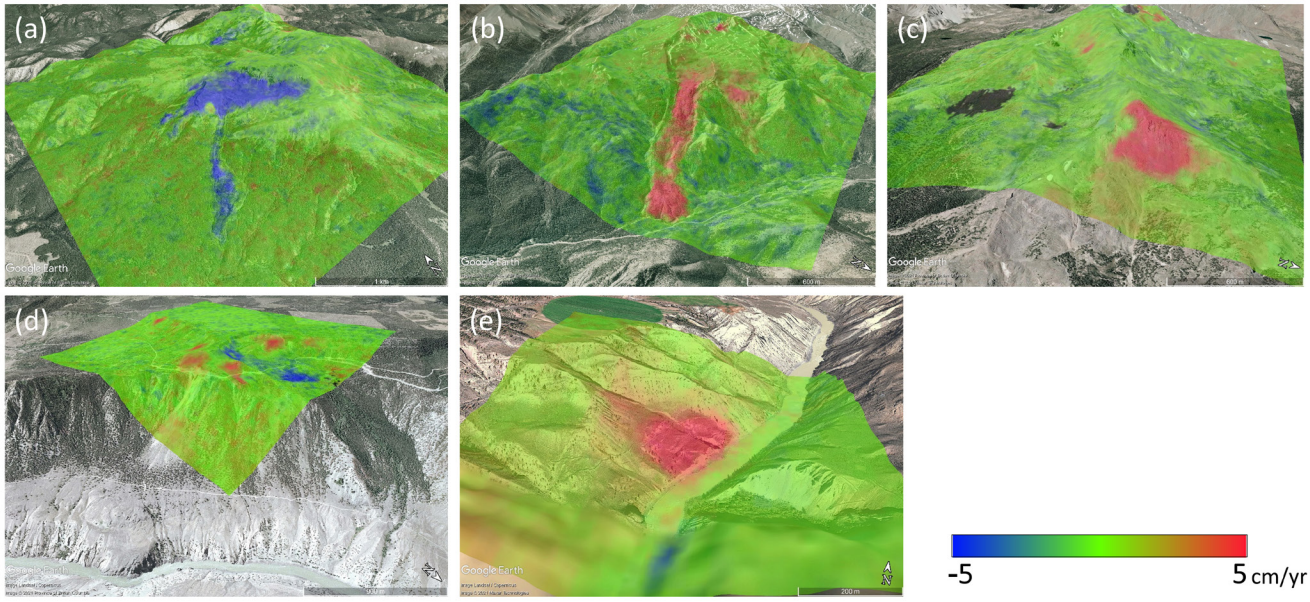

Figure 3. Sentinel-1 linear deformation rate map of east-west movements during 20171008-20210613 rendered on Google Earth imagery, modified from Choe et al. (2021). (a) Site 4 (i.e. Red Mountain), (b) Site 5 (i.e., Yalakom River), (c) Site 6, (d) Site 8, and (e) Site 9 in Choe et al. (2021), respectively.

4. 2. Near Valemount, BC

We observed distinct slope movements with RCM between August and September in 2020 (Figure 4a). With Sentinel-1 we also observed some fringes over a similar period, which are not as distinct as detected from RCM (Figure 4b). More RCM data including 4-day revisit InSAR pairs were acquired during the summer 2021. The time-series linear deformation rate map showed slope movements from the same area (Figure 4c).

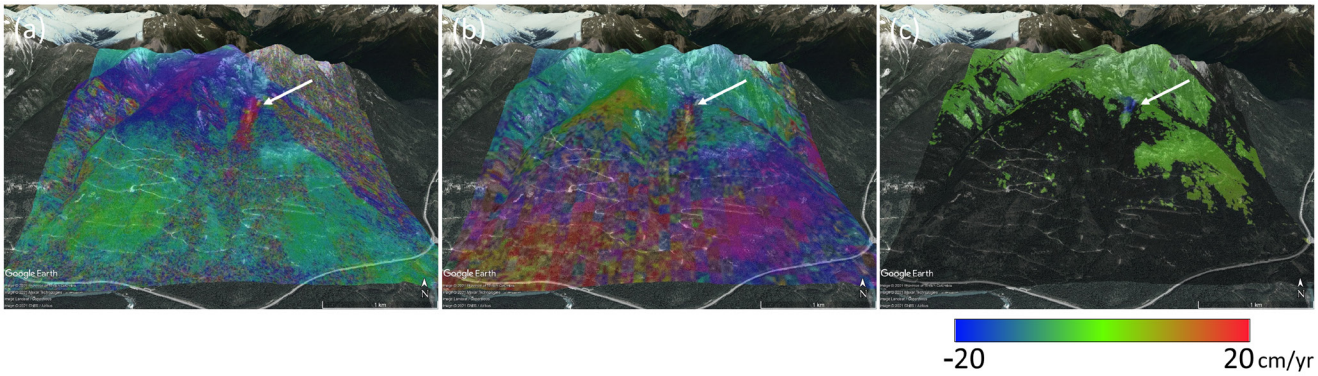

Figure 4. (a) RCM (3M18) DInSAR interferogram of 20200830-20200911. (b) Sentinel-1 DInSAR interferogram of 20200824-20200905. (c) RCM (3M18) linear deformation rate map of line-of-sight movements during 20210613-20210917. The white arrows point to potential slope movements.

4. 3. Mount Currie, BC

Some fringes were observed in the interferograms from lower alluvial fans with the potential of debris flows in Mount Currie area with RCM summer 2020 and 2021 acquisitions (Figures 5a and 5b), while they appeared noisy from Sentinel-1 (Figure 5c). However, C-band (~5.6 cm in

wavelength) InSAR is not applicable to most of surrounding slopes covered by vegetation due to very poor InSAR coherence. Longer wavelength SAR sensors, such as L-band (~24 cm) and P-band (~72 cm), are recommended for monitoring slope movements in these vegetated areas.

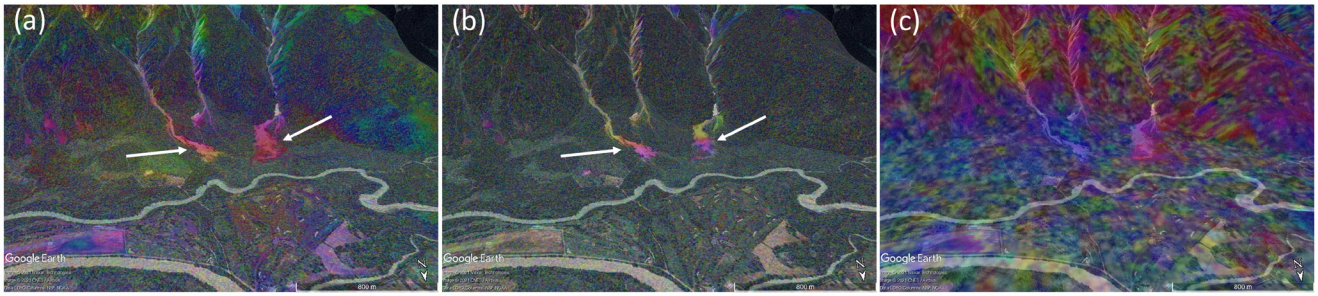

Figure 5. (a) RCM (3M22) DInSAR interferogram of 20200615-20200627. (b) RCM (3M22) DInSAR interferogram of 20210618-20210918. (c) Sentinel-1 DInSAR interferogram of 20200623-20200717. The white arrows point to potential slope movements.

4. 4. Near Pavilion, BC

We did not observe distinct slope movement at the Pavilion earthflow (Bovis, 1985; Bovis and Jones, 1992). However, we detected distinct slope movements with RCM interferograms near the Pavilion earthflow (Figure 6a), which were also confirmed from a RADARSAT-2 linear deformation rate map produced with ~3 year time-series data from December 2015 to October 2018 (Figure 6b). These slope movements were not observed with Sentinel-1 time-series data from October 2017 to June 2021 (Figure 6c). Compared to very-high-resolution RCM of 3 m and spotlight RADARSAT-2 of 1 m, the coarse resolution Sentinel-1 can be limited in detecting smaller slope movements.

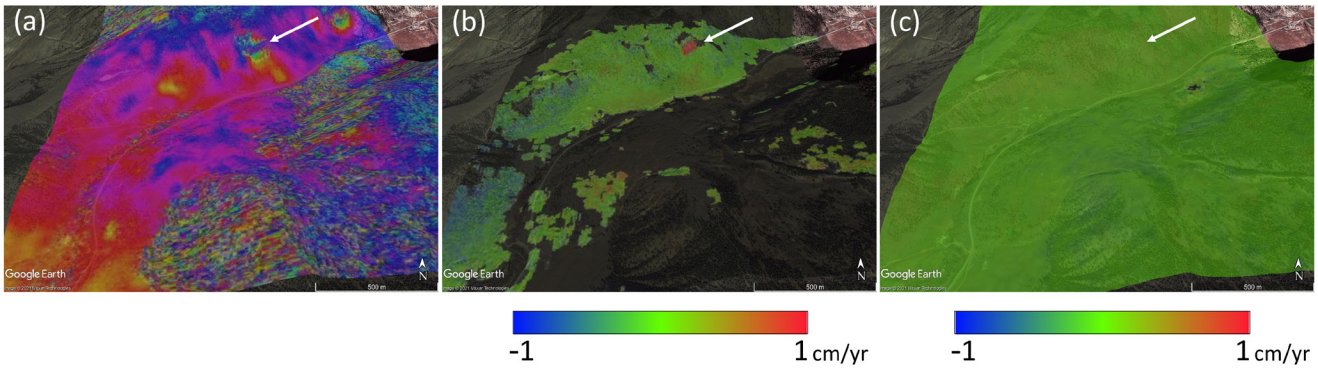

Figure 6. (a) RCM (3M4) DInSAR interferogram of 20210507-20210622. (b) RADARSAT-2 (U79) linear deformation rate map of LOS movements during 20151221-20181018. (c) Sentinel-1 linear deformation rate map of east-west movements during 20171008-20210613. The white arrows point to potential slope movements.

4. 5. Near Quesnel, BC at Big Slide

With RCM, we observed distinct small fringes along a meander of the Fraser River at alandslide called Big Slide and its surrounding slopes near Quesnel (Figures 7a and 7c, August 2020 and April 2021). Fringes were also distinct from the upper parts of the slopes towards the meander during

winter (Figure 7b, February 2021), though these are likely due to snow and ice dynamics. On the other hand, no distinct fringes were observed with Sentinel-1 (Figure 7d, August 2020).

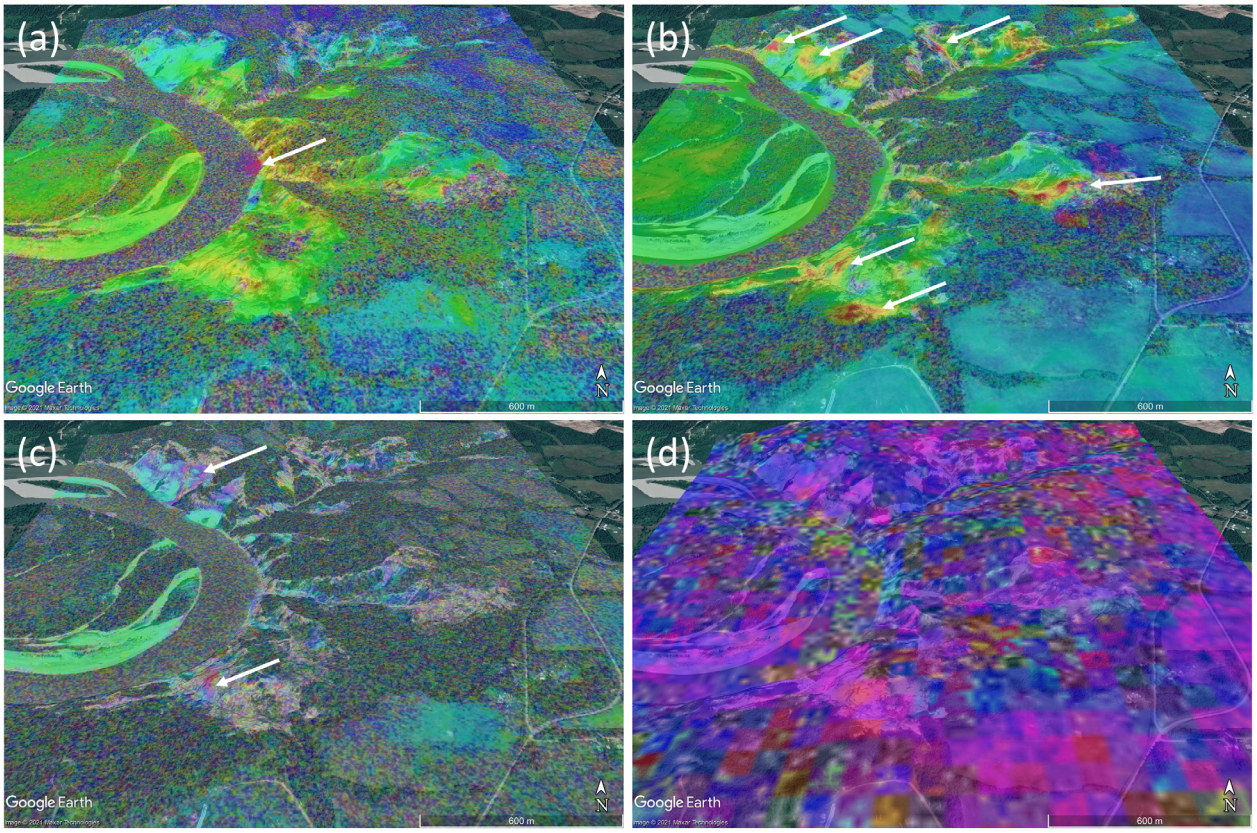

Figure 7. (a) RCM (3M26) DInSAR interferogram of 20200816-20200824. (b) RCM (3M14) DInSAR interferogram of 20210211-20210215. (c) RCM (3M14) DInSAR interferogram of 20210416-20210428. (d) Sentinel-1 DInSAR interferogram of 20200816-20200828. The white arrows point to potential slope movements.

4. 6. Texas Creek, BC

With RCM interferograms, we observed fringes from slopes (Figure 8a) and LOS movements with time-series acquisitions over ~4 months in summer 2021 (Figure 8b). However, most of the surrounding areas showed low coherence, which could be the result of discontinuity and uncertainty in the phase unwrapping process.

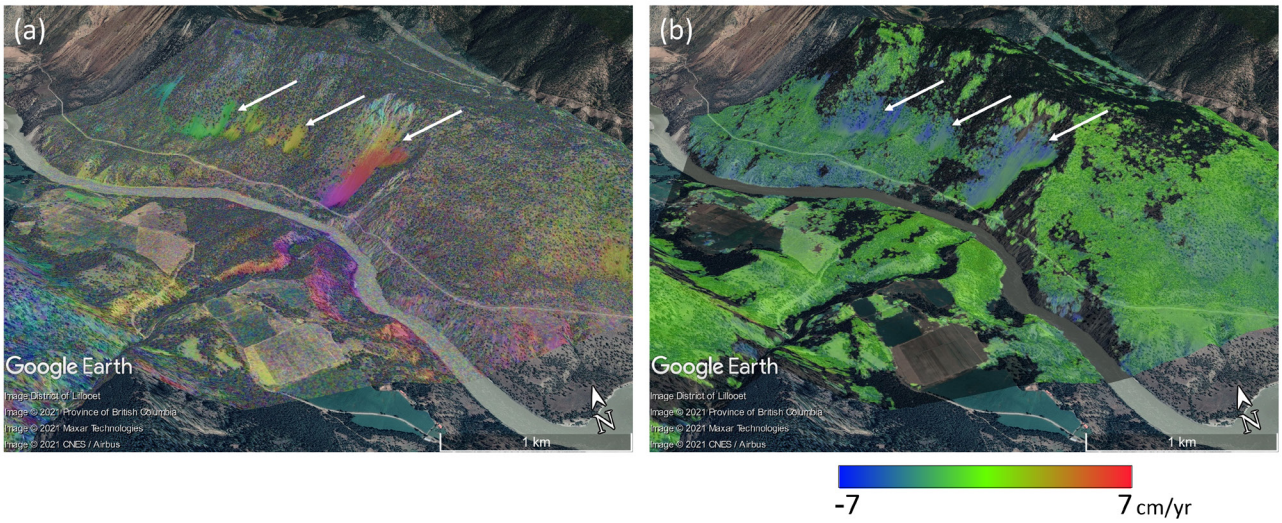

Figure 8. (a) RCM (3M28) DInSAR interferogram of 20210727-20210808. (b) RCM (3M28) linear deformation rate map of LOS movements during 20210512-20210913. The white arrows point to potential slope movements.

4. 7. Harrison Lake, BC

The RCM imagery acquired at a low incidence angle (~19°) showed very poor coherence due to the layover effect from the steep slopes in Harrison Lake North (Figure 9a). The RCM acquired at a high incidence angle (~42°), on the other hand, mitigated the geometric distortion and could obtain coherent signals from some well-exposed slope surfaces (Figure 9b), though most areas still showed low coherence due to vegetation. Thus, in the case of steep slopes, it is important to select an optimal incidence angle depending on the slope gradient. Harrison Lake South is difficult to monitor due to very low coherence caused by vegetation. (Figure 10).

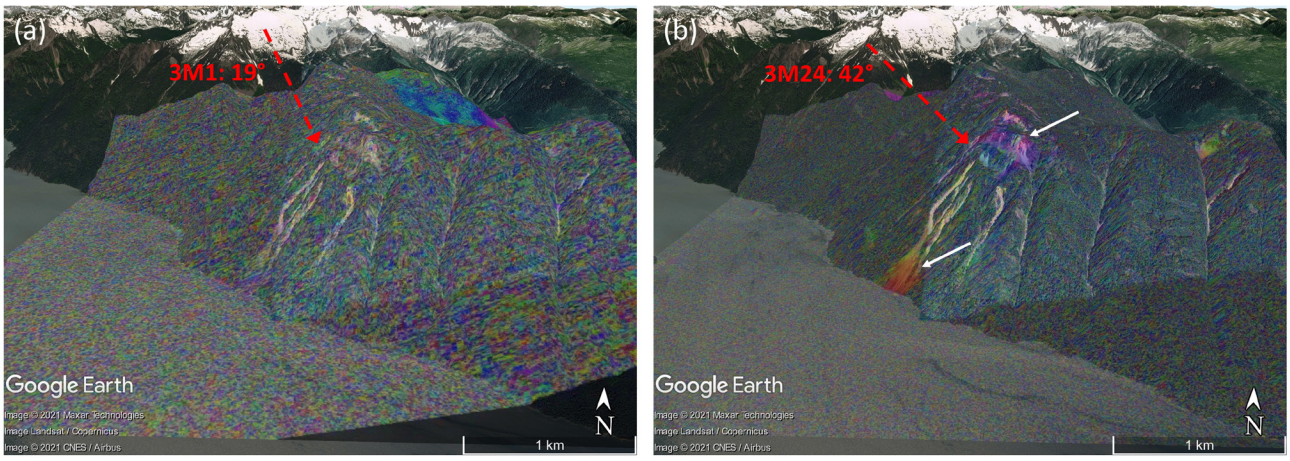

Figure 9. Harrison Lake North. (a) RCM (3M1) DInSAR interferogram of 20200830-20200903. (b) RCM (3M24) DInSAR interferogram of 20210604-20210718. The red arrows represent the SAR looking directions. The white arrows point to potential slope movements.

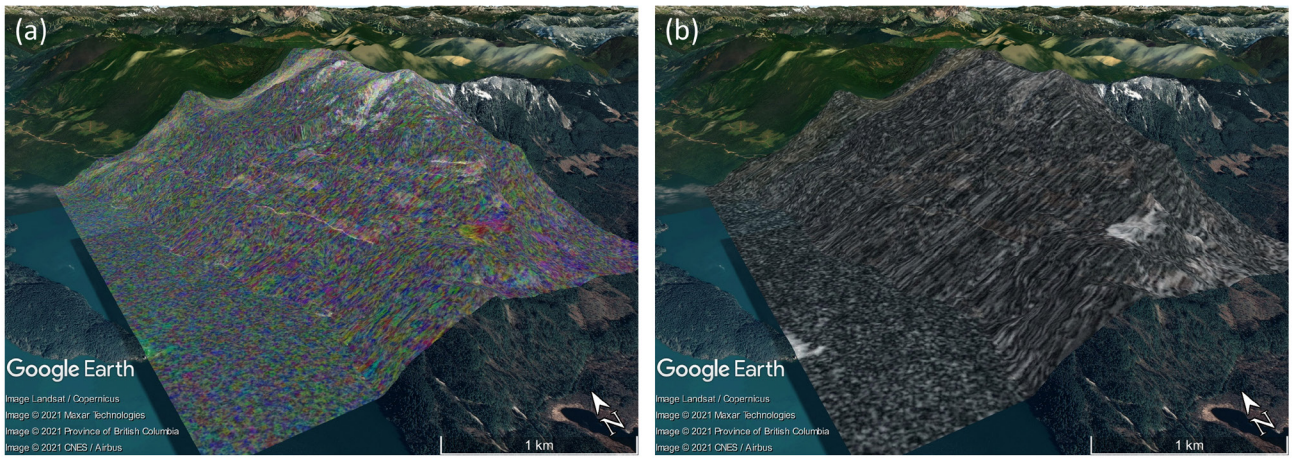

Figure 10. Harrison Lake South. (a) RCM (3M26) DInSAR interferogram of 20200821-20200902. (b) Coherence of 20200821-20200902, ranging from 0 (black) to 1 (white).

4. 8. Chilliwack, BC

The vegetated slopes in the Chilliwack area are difficult to monitor with C-band due to very low coherence (Figure 11).

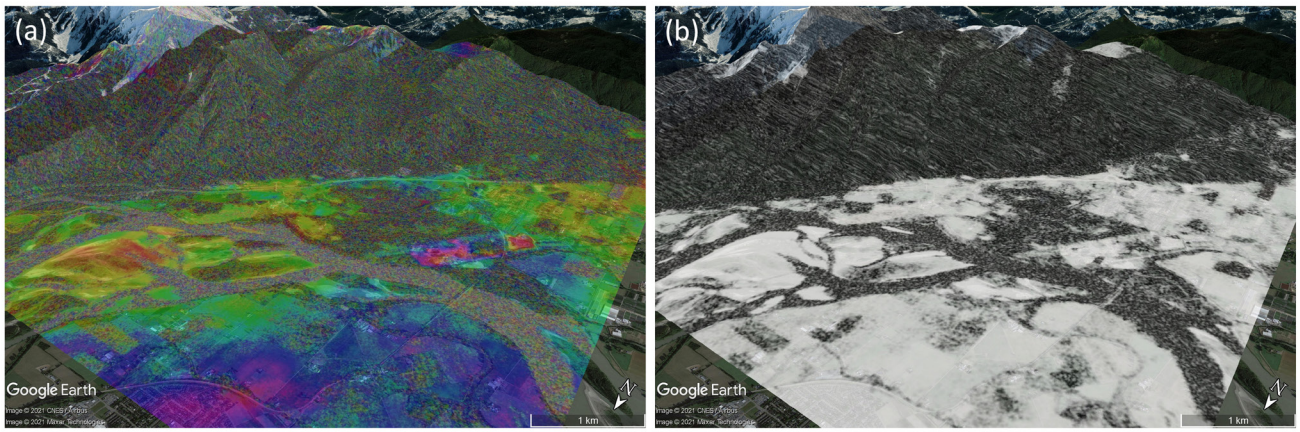

Figure 11. (a) RCM (3M2) DInSAR interferogram of 20210826-20210930. (b) Coherence of 20210826-20210930, ranging from 0 (black) to 1 (white).

4. 9. Near Mystery Creek rock avalanche, BC

No distinct fringes were observed from this area. However, acquiring imagery was also difficult, which limited possible comparisons in time.

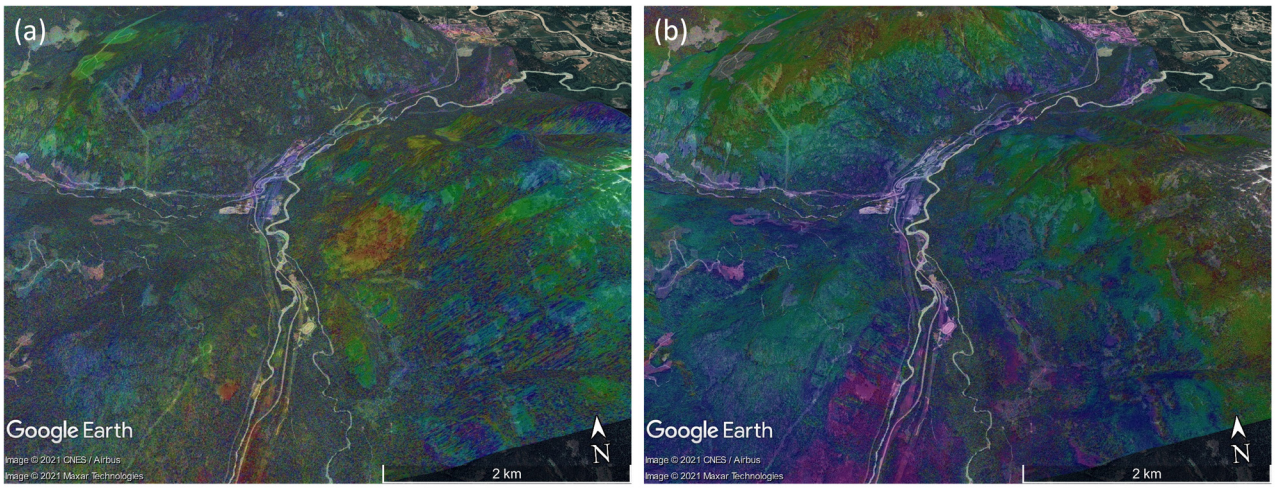

Figure 12. (a) RCM (3M20) DInSAR interferogram of 20200711-20200824. (b) RCM (3M22) DInSAR interferogram of 20210509-20210521.

4. 10. Near Nimbus Mountain, BC

Compared to the RADARSAT-2 24-day pair (Figure 13a) acquired over a similar period, the RCM 4-day pair (Figure 13b) showed much better coherence. However, it is challenging to detect movements from vegetated steep slopes in Nimbus Mountain (Figure 13c).

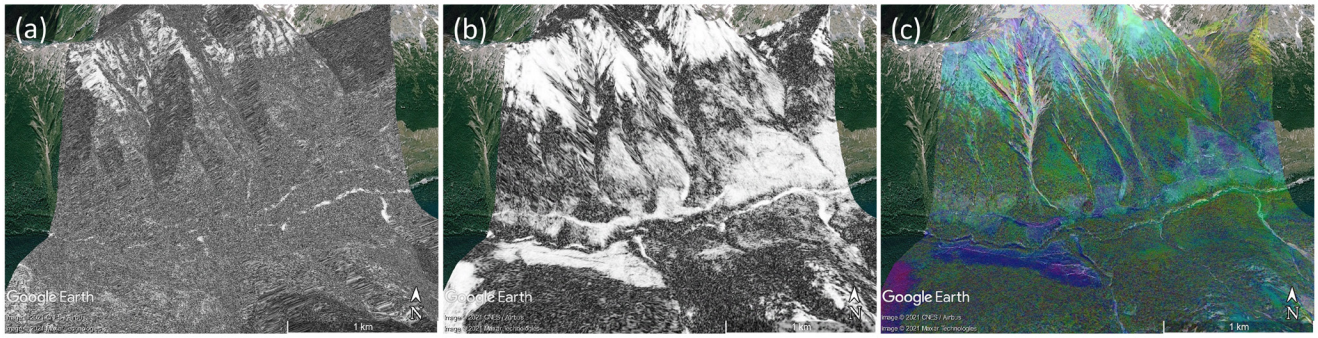

Figure 13. (a) RADARSAT-2 (U1) coherence of 20200529-20200622. (b) RCM (3M34) coherence of 20200524-20200528. (c) RCM (3M34) DInSAR interferogram of 20200524-20200528.

4. 11. Lions Bay, BC

Only 4 RCM images were acquired with the 1 m spotlight mode in May and June, 2020. Some fringes showing potential slope movements were observed from upper slopes (i.e., north flank of Harvey Creek drainage basin), but these are not certain because of the very limited number of acquisitions. More acquisitions are needed to confirm the potential movement. However, steep slopes and vegetation are obstacles.

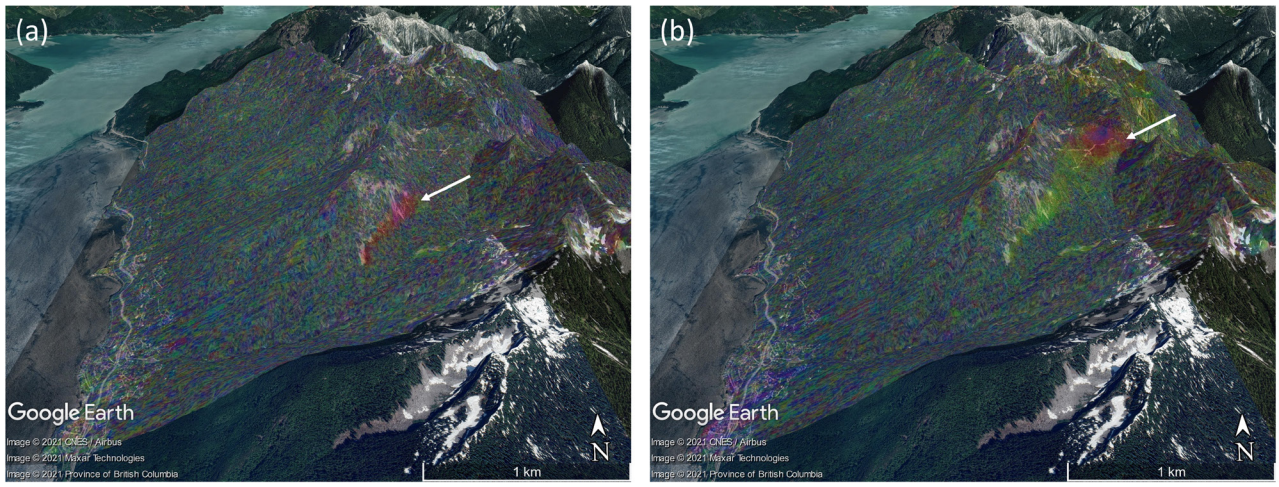

Figure 14. (a) RCM (FSL5) DInSAR interferogram of 20200515-20200624. (b) RCM (FSL5) DInSAR interferogram of 20200620-20200624.

4. 12. Kicking Horse, BC

RCM acquisitions were acquired only during the winter season (2021). Observed fringes are likely to be related to snow and ice dynamics.

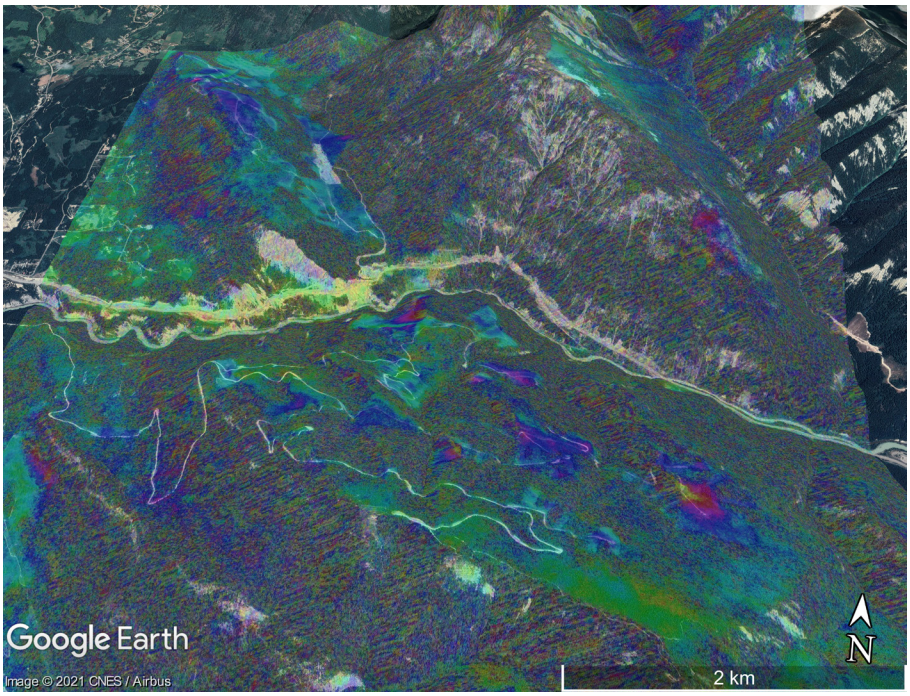

Figure 15. RCM (3M10) DInSAR interferogram of 20210107-20210111.

4. 13. Swan Hills, AB

With RCM, we detected potential slope movements over ~4 months in summer 2021 (Figure 16).

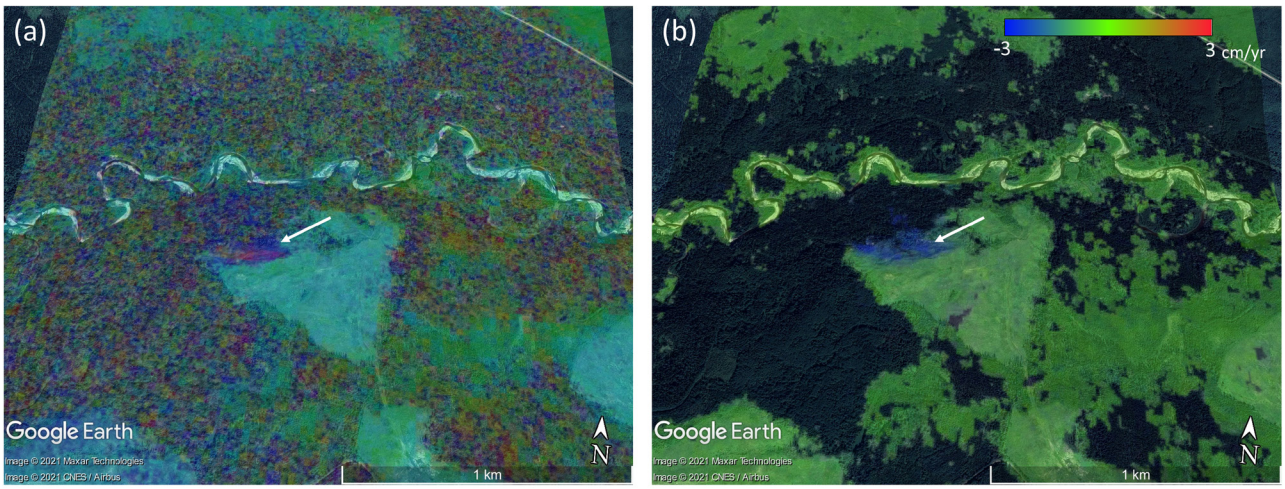

Figure 16. (a) RCM (5M12) DInSAR interferogram of 20210911-20210919. (b) RCM (5M12) linear deformation rate map of LOS movements during 20210510-20210927. The white arrows point to potential slope movements.

4. 14. Freeman River, AB

RCM DInSAR fringes were observed only from ponds and swamps in the Freeman River area (Figure 17).

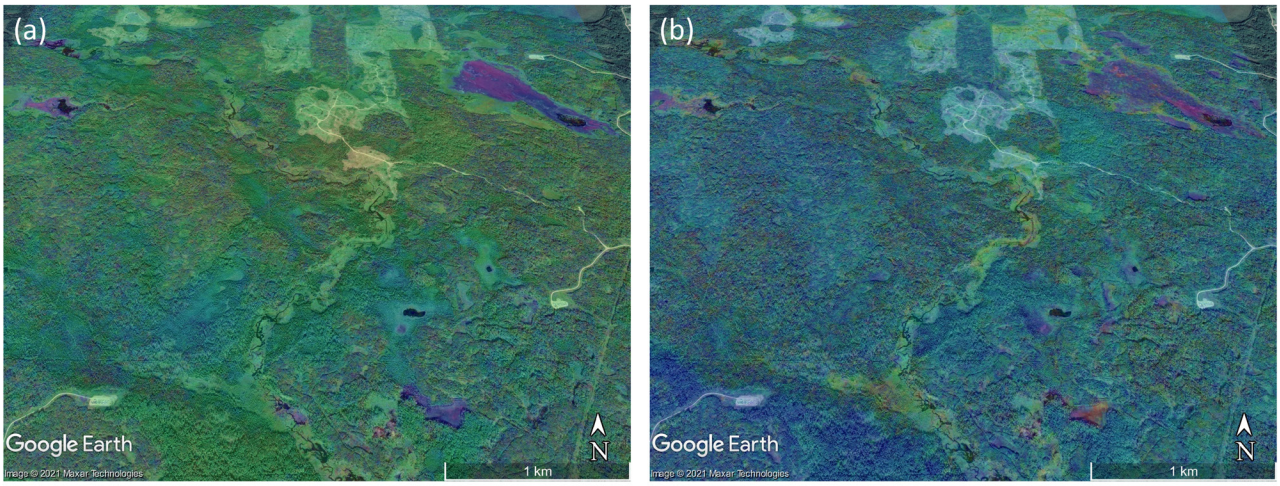

Figure 17. (a) RCM (VH15) DInSAR interferogram of 20200908-20200912. (b) RCM (5M5) DInSAR interferogram of 20201218-20201230.

4. 15. Pangnirtung, NU

Figure 18 shows DInSAR observations from RADARSAT-2, Sentinel-1, and RCM. Fringes were observed mostly along the valley towards the community and inlet in northwest.

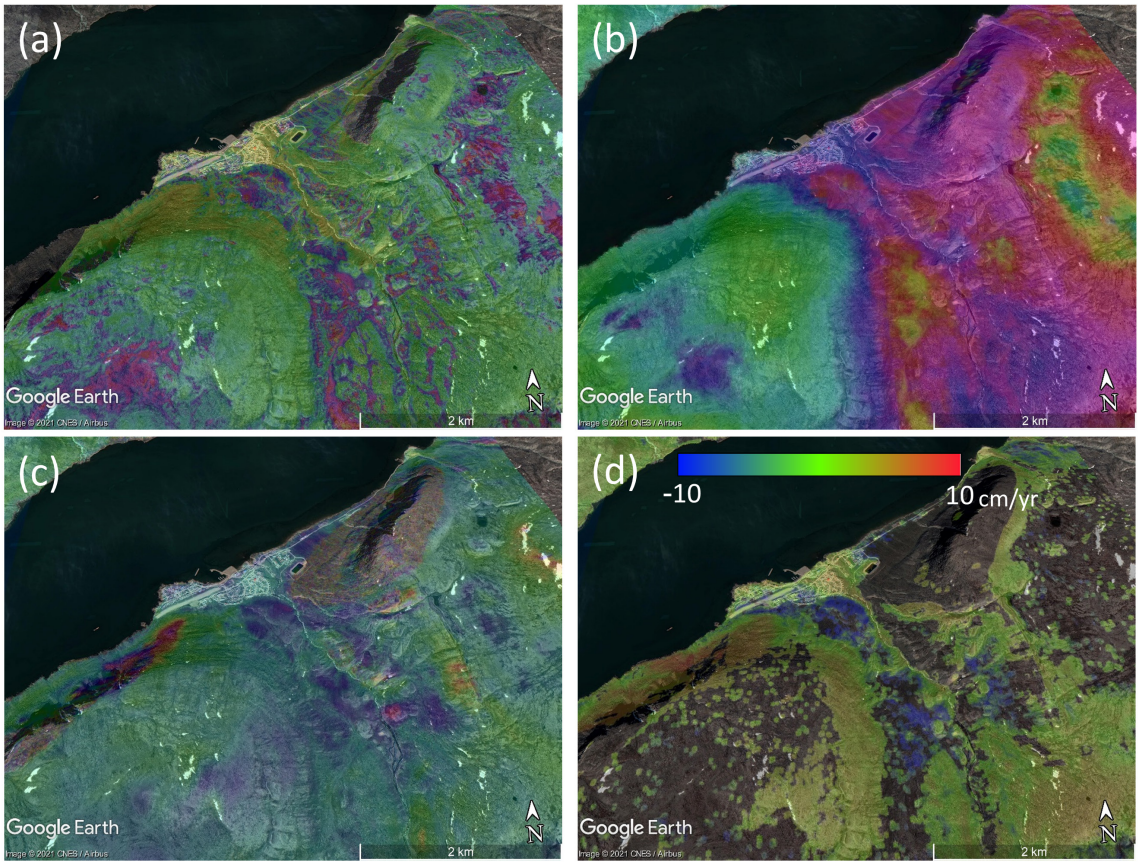

Figure 18. (a) RADARSAT-2 (SLA25) DInSAR interferogram of 20190819-20190912. (b) Sentinel-1 DInSAR interferogram of 20190812-20190824. (c) RCM (3M1) DInSAR interferogram of 20210820-20210824. (d) RCM (3M1) linear deformation rate map of LOS movements during 20210601-20210925.

4. 16. Bylot, NU

Very small fringes within a few hundred metres were sporadically observed along the slopes on Bylot Island during summers 2020 (Figure 19a) and 2021 (Figure 19b).

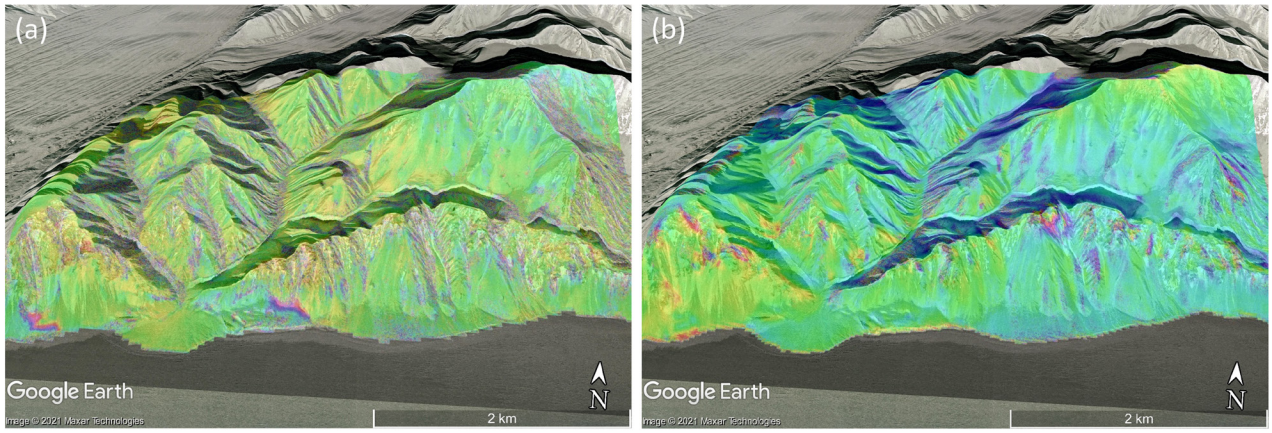

Figure 19. (a) RCM (3M38) DInSAR interferogram of 20200624-20200819. (b) RCM (3M36) DInSAR interferogram of 20210801-20210821.

4. 17. Coronation, NU

Coronation shows great examples of glacier movements in summer (Figure 20a) and winter (Figure 20b) observed with RCM 4-day revisit pairs.

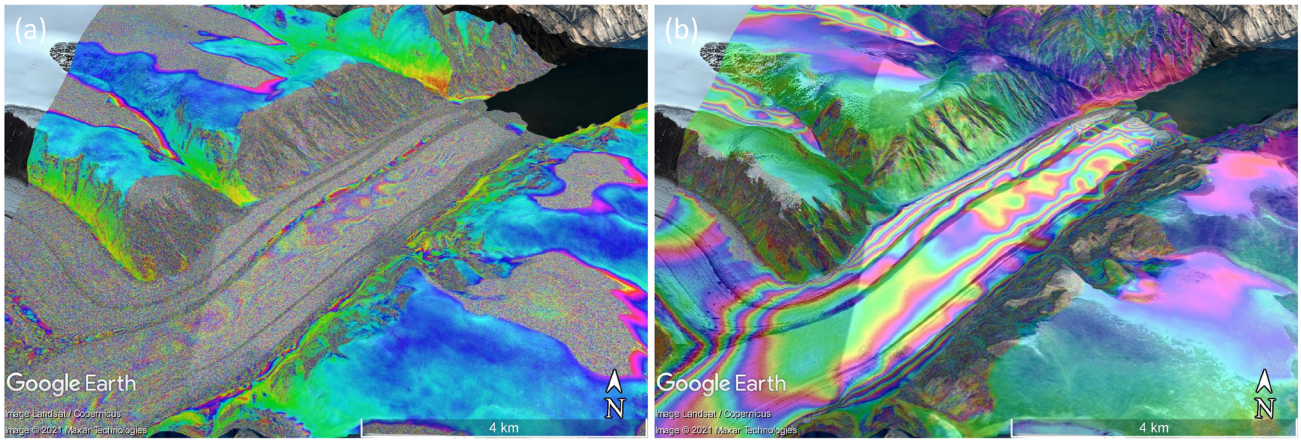

Figure 20. (a) RCM (3M10) DInSAR interferogram of 20200826-20200830. (b) RCM (3M13) DInSAR interferogram of 20210121-20210125.

4. 18. Southwind, Clyde River, Grise Fiord, NU

Some fringes were observed with RCM 8-day (Figure 21a) and 4-day (Figures 21b and 21c) InSAR pairs, but more time-series acquisitions are needed to confirm slope movements.

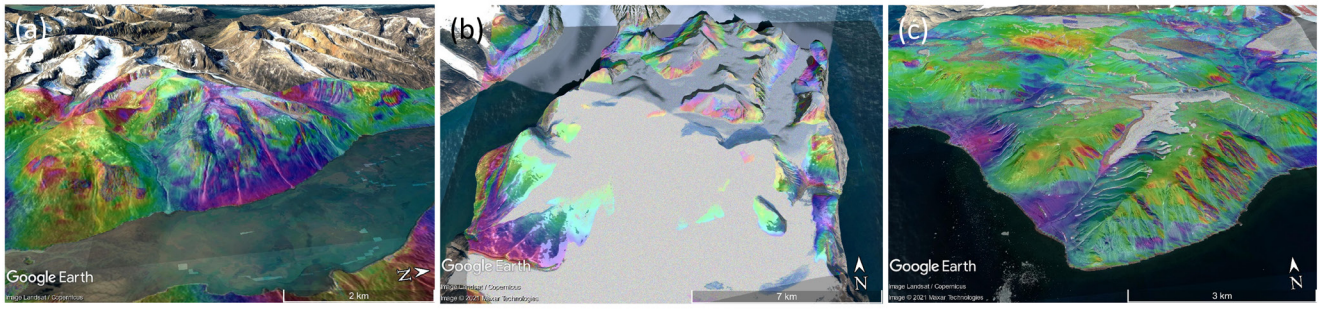

Figure 21. (a) Southwind, RCM (3M28) DInSAR interferogram of 20200818-20200826. (b) Clyde River, RCM (3M31) DInSAR interferogram of 20200815-20200819. (c) Grise Fiord, RCM (3M18) DInSAR interferogram of 20200627-20200701.

5. Summary

RCM InSAR preliminary observations showed great potential for monitoring more detailed slope movements with higher spatial and temporal resolutions, compared to C-band imagery from Sentinel-1 and RADARSAT-2. However, C-band results are limited to well-exposed surfaces due to low coherence in areas that are densely vegetated. L- and P-band SAR with a capability to penetrate vegetation with a longer wavelength are recommended for monitoring slope movements over vegetated areas. For steep slopes, optimal incidence angles should be selected by considering the slope and aspect of target surfaces. Sentinel-1 time-series analyses at a regional scale also can be helpful for planning new RCM acquisitions at a local scale.

Acknowledgments

The authors would like to thank D. Huntley for comments and suggestions that have greatly improved the manuscript. In addition, P. Friele and A. Normandeau are thanked for contributing to the list of sites that should be monitored.

References

Blais-Stevens, A. (2020) Historical landslides that have resulted in fatalities in Canada (1771-2019); Geological Survey of Canada, Open File 8392; doi.org/10.4095/326167.

Blais-Stevens, A. (2022) Landslides that have resulted in fatalities in Canada (1771-2022), Geological Association of Canada Annual Meeting, Abstracts and Programs, Special Session 20.

Bovis, M.J. (1985) Earthflows in the Interior Plateau, southwest British Columbia. Can. Geotech. J, 22, 313-334.

Bovis, M.J.; Jones, P. (1992) Holocene history of earthflow mass movements in south-central British Columbia: The influence of hydroclimatic changes. Can. J. Earth Sci., 29, 1746-1755.

Choe, B.-H.; Blais-Stevens, A.; Samsonov, S.; Dudley, J. (2021) Sentinel-1 and RADARSAT Constellation Mission InSAR assessment of slope movements in the Southern Interior of British Columbia, Canada. Remote Sens., 13, 3999. https://doi.org/10.3390/rs13193999

CBC News a) November 17, 2021 B.C. declares state of emergency in wake of devastating flooding, mudslides; CBC News, https://www.cbc.ca/news/canada/british-columbia/wyntk-bc-floods-nov-17-1.6251839.

CBC News b), June 29, 2021 High temperatures push western wildfire risk into uncharted territory; https://www.cbc.ca/news/canada/edmonton/heat-wildfires-1.6084114.

CBC News c) June 19, 2021 Uguen-Csenge, E.; Lindsay, B. For 3rd straight day, B.C. village smashes record for highest Canadian temperature at 49.6 °C; https://www.cbc.ca/news/canada/british-columbia/bc-alberta-heat-wave-heat-dome-temperature-records-1.6084203.

CTV News Vancouver, 1 July 2021, Scientists warn extreme heat wave that preceded Lytton fire may not be isolated event https://bc.ctvnews.ca/scientists-warn-extreme-heat-wave-that-preceded-lytton-fire-may-not-be-isolated-event-1.5493667

Dudley, J.P.; Samsonov, S.V. (2020) The Government of Canada automated processing system for change detection and ground deformation analysis from RADARSAT-2 and RADARSAT Constellation Mission Synthetic Aperture Radar data: description and user guide; Geomatics Canada, Open File 63.

Porter, M.; Van Hove, J.; Barlow, P.; Froese, C.; Bunce, C.; Skirrow, R.; Lewycky, D.; Bobrowsky, P.T. (2019) The estimated economic impacts of Prairie landslides in western Canada. In Proceedings of the 72nd Canadian Geotechnical Conference; Paper 308, St. John's, Newfoundland and Labrador.

Singhroy, V.; Fobert, M.-A.; Li, J.; Blais-Stevens, A.; Charbonneau, F.; Das, M. (2020) Advances in Remote Sensing for Infrastructure Monitoring. In: Advances in radar images for monitoring Transportation, Energy, Mining and Coastal Infrastructure, V. Singhroy (ed.), Springer: 3-40. doi.org/10.1007/978-3-030-59109-0_1.

Appendix. RCM data acquisitions used in this work

Site	*Coordinates (Lat, Lon)*	*RCM mode (ASC)*	*Start-End date*	*N (ASC)*	*RCM mode (DES)*	*Start-End date*	*N (DES)*
Valemount, BC	53.00, -119.34	3M10	20200411+	64+	3M8	20200408-20210411	29
		3M22	20200408-20210626	33	3M18	20200407+	56+
Lions Bay, BC	49.45, -123.23	FSL5	20200413-20200624	4			
Mystery Creek, BC	50.18, -122.87	3M20	20200410-20200824	3	3M34	20200411-20200329	19
Nimbus Mountain, BC	54.20, -128.10	3M10	20200501-20200724	6	3M34	20200418-20210328	29
Quesnel, BC	53.08, -122.52	3M26	20200512+	28+	3M14	20200515+	34+
Chilliwack, BC	49.14, -121.80	3M13	20200620+	15+	5M21	20200613-20210612	23
Texas Creek, BC	50.57, -121.79	3M4	20201212+	12+	3M28	20210410+	14+
Harrison Lake N, BC	49.65, -121.94	3M24	20210119+	16+	3M5	20210118-20210623	17
Harrison Lake S, BC	49.38, -121.73	3M2	20200528+	31+	3M26	20210402-20210613	7
Yalakom River, BC	51.06, -122.49	3M2	20200518+	47+	5M18	20200622+	40+
		3M12	20200620+	29+	5M23	20200613+	47+
Pavilion, BC	50.87, -121.81	3M4	20200514-20210622	6	3M40	20200512-20200520	3
Mount Currie, BC	50.29, -122.77	3M21	20200816-20210616	8	3M22	20200518+	17+
					3M34	20200411-20210329	19
Kicking Horse, BC	51.30, -116.90	3M10	20201206-20210127	10	3M24	20201127-20210327	25
Swan Hills, AB	54.71, -115.40	5M19	20200724+	46+	5M12	20200726+	62+
Freeman River, AB	54.40, -114.93	VH15	20200714-20210130	14	5M5	20200727-20210328	33
		3M15	20210126-20210315	6	5M10	20210315-20210327	3
Bylot, NU	72.90, -77.98	3M34	20200603-20210614	21	3M30	20200604+	32+
		3M38	20200604-20210713	21	3M36	20200705+	31+
Pangnirtung, NU	66.14, -65.70	3M1	20210108+	31+	3M3	20210102-20210327	12
					3M10	20200830-20210614	9
Southwind, NU	66.67, -62.40	3M7	20210107-20210119	3	3M28	20200818-20210109	5
		3M21	20210121-20210318	2			
Coronation, NU	67.19, -64.84	3M13	20200603-20210318	8	3M10	20200611-20210330	28
Grise Fiord, NU	76.41, -82.85	3M41	20200618-20210225	16	3M18	20200627-20210330	26
Clyde River, NU	70.42, -71.28	3M31	20200706-20210303	27	3M4	20200812-20210328	38
		3M34	20200819-20210126	7	3M13	20200810-20210330	48
					3M41	20200816-20210328	15

* Date format: YYYYMMDD; +: acquisitions on-going; ***N***: acquisition number (up-to-date: 20210930).